



## An experimental study of vapor bubbles dynamics at water and ethanol pool boiling at low and high heat fluxes

Anton Surtaev <sup>a,b,\*</sup>, Vladimir Serdyukov <sup>a,b</sup>, Jingjing Zhou <sup>c</sup>, Aleksandr Pavlenko <sup>a</sup>, Vladislav Tumanov <sup>a,b</sup>

<sup>a</sup> Kutateladze Institute of Thermophysics, 1 Lavrentiev ave., Novosibirsk, Russia

<sup>b</sup> Novosibirsk State University, 2 Pirogov str., Novosibirsk, Russia

<sup>c</sup> School of Chemical Engineering and Technology, Tianjin University, 135 Yaguan Road, Tianjin, China



### ARTICLE INFO

#### Article history:

Received 7 March 2018

Received in revised form 21 May 2018

Accepted 1 June 2018

Available online 14 June 2018

#### Keywords:

Pool boiling

Liquid microlayer

Dry spots

Heat transfer

Two-phase flows

High speed visualization

IR thermography

### ABSTRACT

In this paper the results of experimental study of vapor bubbles dynamics at pool boiling of various liquids in a wide range of heat fluxes up to  $q/q_{CHF} \sim 0.9$  are presented. The experiments were performed at boiling of saturated water and ethanol at atmospheric pressure with the use of high-speed experimental techniques including video macro-visualization and IR thermography from the bottom side of a transparent heated sample. As a result, new data on the growth rate of vapor bubbles and dry spots in their base, evolution of the liquid microlayer region and unsteady temperature field of a thin film heater surface were obtained, and analysis of patterns of process at low heat fluxes was carried out. The usage of high-speed experimental techniques also allowed in this study to investigate the evolution of vapor bubbles with formation of vapor patterns and large agglomerates, to study dry spots dynamics, to estimate void fraction close to heating surface at fully developed nucleate boiling regime up to the critical heat flux depending on liquid properties. Obtained experimental information can be further used to construct more accurate physical models for the theoretical description of microcharacteristics, heat transfer and boiling trigger mechanisms at nucleate boiling of liquids with different physical properties.

© 2018 Elsevier Ltd. All rights reserved.

## 1. Introduction

Since first papers of Moore and Mesler [1], Labuntsov [2] and Cooper and Lloyd [3], in which authors have proposed the hypothesis of rapidly evaporating thin liquid film at the base of a vapor bubble to explain the sharp decrease in the local temperature at the moment of vapor bubble appearance, the phenomena of the microlayer and influence of its evaporation dynamics on heat transfer at nucleate boiling are widely discussed in the literature [4–6]. At the same time, the detailed picture, based on the experimental data on the microlayer dynamics, its characteristics, including thickness, evaporation rate, etc., has not been available to date. The complexity of such studies is related to the fact that the characteristic thickness of microlayer is several microns and the process of its formation and development does not exceed few milliseconds.

Nowadays, high-speed video recording from the side of the heater is common and already classical technique of nucleate boiling visualization. This type of recording allows to study the evolution of vapor bubbles shape, to measure their departure diameters

and nucleation frequencies. So nowadays there are a lot of works devoted to experimental investigation of the vapor bubbles dynamics at pool boiling of various liquids on surfaces with different orientation, geometry and roughness, at various pressures and subcooling degree [7–9]. However video recording from the side of a heater has a number of shortcomings. Among them are the impossibility of observing the sizes of microlayer evaporation region and dry spot, formed at the bubble growth stage in a nucleation site, the impossibility of microlayer thickness determination. Moreover, activation of significant number of nucleation sites, even at relatively low heat fluxes, makes it difficult to identify individual vapor bubbles. This significantly increases the measurement error and complicates analysis of the nucleation dynamics at boiling in a wide range of heat fluxes.

The development of modern experimental techniques in the last two decades makes it possible to obtain fundamentally new information on local and integral characteristics of boiling, including heat transfer coefficient and critical heat flux. Nowadays one of the most popular noninvasive methods to measure the non-stationary temperature field of the heating surface is high-speed infrared (IR) thermography. First, who have used this method for boiling process investigation, were Theofanous et al. [10,11]. In these and subsequent papers [12–15], it was shown, that the usage

\* Corresponding author.

E-mail address: [surtaev@itp.nsc.ru](mailto:surtaev@itp.nsc.ru) (A. Surtaev).

## Nomenclature

$A$	area	$\gamma, \beta$	empirical constants
$C_{sf}$	constant for surface fluid term	$\delta$	thickness
$D$	diameter	$\rho$	density
$g$	gravity constant	$\sigma$	surface tension
$h$	distance		
$h_{av}$	cooling depth		
$h_{fg}$	latent heat of vaporization		
$I$	current		
$Ja$	Jacob number		
$k$	thermal conductivity		
$q$	heat flux density		
$R$	radius		
$R_a$	surface roughness		
$T$	temperature		
$t$	time		
$u$	velocity		
$V$	voltage		
$\Delta T$	wall superheat		
<i>Subscripts</i>			
$a$	ascent rate		
$CHF$	critical heat flux		
$dep$	departure		
$ds$	dry spot		
$ev$	evaporation		
$g$	bubble growth		
$l$	liquid		
$ml$	microlayer		
$o$	outer		
$sat$	saturation		
$v$	vapor		
$w$	wall; bubble waiting		

### Greek symbols

$\alpha$	thermal diffusivity
----------	---------------------

of high-speed IR thermography allows to measure bubble nucleation temperature, nucleation site density and frequency, etc. In [16,17] with the use of this method the evolution of temperature field under single bubble was obtained, on the basis of which the features of the local heat transfer in regions of microlayer and dry spot were studied. Also researchers have actively used laser interferometry technique to study the geometry and dynamics of the liquid microlayer at boiling of various liquids [4,18–21]. The laser interferometry technique allows not only to determine the sizes of microlayer and dry spots regions, but also to measure microlayer thickness evolution at the bubble growth stage. Therefore, development and further usage of modern experimental techniques allows to obtain fundamentally new information on the multiscale characteristics of nucleate boiling. However, literature analysis shows that existing experimental data on local boiling characteristics, especially those taking place in the region of triple contact line, are insufficient for theoretical description of the microlayer characteristics, its evolution and evaporation rate at boiling of liquids with various physical properties under different conditions, including pressure change.

In addition to the partially nucleate boiling regime, the nucleation dynamics and evolution of two-phase layer close to heating wall at developed nucleate boiling up to crisis phenomena development (CHF) also has a great interest and importance. Such interest is related both with incomplete understanding of basic heat transfer mechanisms at boiling in the region of high heat fluxes, and with the necessity to determine the main reasons of boiling crisis phenomena development, including modeling safe operation of nuclear reactors [23]. Many researchers have attempted to theoretically describe trigger mechanisms of CHF on the basis of the evolution of liquid-vapor system at developed nucleate boiling. Such approaches can be attributed to the already classic Kutateladze-Zuber hydrodynamic instability model and number of its modifications, as well as subsequent semi-empirical models, which are described in detail in recent reviews [24–26]. At the same time, existing experimental observations do not yet provide a clear picture and understanding of the characteristics and evolution of the two-phase system close to a heating surface at pool boiling of liquids with various properties in the region of high heat fluxes.

In one of the first papers [27], devoted to an experimental study of vapor bubbles dynamics at developed nucleate boiling, author

observed formation of large-scale vapor agglomerates (or “vapor mushrooms”), which were anchored to a heating surface by numerous columnar stems of vapor. However, due to the appearance of a large number of vapor bubbles at high heat fluxes, performed photographic study from the side of a flat heater did not allow author to firmly reiterate this assumption, which was later noted in [11]. Kirby and Westwater [28] and later Van Ouwerkerk [29] with the use of transparent conductive heaters visualized nucleate boiling at various pressures directly from bottom side of the heaters, which made it possible to study in detail the formation and growth of dry spots under single vapor bubbles up to CHF point. As a result, the existence of a thin liquid layer close to a heating wall, which was later called the liquid “macrolayer”, was proposed. In these papers, the hypothesis of the onset of boiling crisis phenomena development as a result of the irreversible dry spots formation and their subsequent lateral growth along a heating surface was also formulated.

Based on the described experimental observations, Katto and Yokoya [30] and further Haramura and Katto [31] proposed a modified hydrodynamic instability model of boiling crisis, which is widely known in the literature as the “macrolayer dryout model”. This model assumes that at developed nucleate boiling, the vapor-liquid system represents stationary columnar stems of vapor, distributed in a thin near-wall liquid macrolayer. The onset of crisis developments corresponds to the moment of complete macrolayer evaporation under massive vapor conglomerate. The hypothesis of liquid rich layer existence close to the heating wall was confirmed by number of researchers [32–36] during experimental investigations on void fraction distribution close to a heating surface at boiling of water, isopropanol and FC-72. Nevertheless, authors of [34] also pointed out that the existence of stationary vapor stems in the liquid macrolayer is rather unlikely.

Chu et al. [37] demonstrated the structure of large vapor agglomerates, as well as the behavior of dry spots formed under them. The experiments were carried out at saturated water boiling on the surface of narrow transparent heater (2.7 mm wide). With the use of synchronized total reflection technique and video recording from the side of the heater authors observed formation of large-scale coagulated dry patch under vapor agglomerates. Authors pointed out, that this fact also directly contradicts macrolayer dryout model.

Authors of [38–40] also used total reflection technique to study dry spots dynamics at developed nucleate boiling of well wetting fluids, such as R-113 and ethanol. Based on the data analysis authors of these works suggested that there are always almost dried up surface under single bubbles. With the increase of input heat flux neighboring bubbles coalesce in a lateral direction with each other and form large vapor conglomerate, which in turn forms coagulated dry area on a heating surface. Authors also noted that near the CHF point the dried up surface area can reach 70% of the total heating surface area. However, studies on dry spots dynamics at water boiling performed with the use of high-speed IR recording [11,41] showed that dry spots occupy a much smaller area in pre-crisis boiling regimes. Crisis phenomena development is a consequence of the appearance of local regions on heating surface with high temperature or irreversible dry spots. In addition, authors of [11] also studied cross-sectional average void fraction as a function of distance from the heater by X-ray radiographic imaging of the boiling liquid volume. Analysis of obtained data showed that void fraction near CHF conditions ( $q/q_{CHF} = 0.8 \div 0.9$ ) at the distances from the heating surface up to 1 mm reaches 90%. Nevertheless, it should be also noted that in this paper the minimum distance from the heating surface, at which void fraction was measured, was 0.5 mm, which in turn, made it impossible to investigate void fraction in the region of liquid rich layer with a thickness of dozens microns [42,43].

Therefore, nowadays in the literature there is limited number of experimental studies devoted to the processes occurring in the region of the triple contact line at liquid boiling. At the same time, experimental data on the microlayer evaporation dynamics, its dimensions and thickness are highly relevant for the development of new and verification of already existing theoretical approaches for describing both local characteristics of nucleation and the intensity of heat transfer at nucleate boiling. A similar situation is observed with the investigations of the characteristics and evolution of two-phase system at nucleate boiling in the range of high heat fluxes. Depending on experimental information, obtained with the use of various techniques, authors describe physical mechanisms in different ways. This is related to the fact that the liquid-vapor system behavior close to the heating surface depends heavily on a number of parameters, such as liquid microhydrodynamics, local heat transfer rate in the area of vapor bubbles, fluid and wall properties, including wetting, pressure and so on. This indicates the need for further experimental study of the behavior of two-phase system close to a heater at developed nucleate boiling of liquids with different physical properties. In this case, one of the most promising techniques for studying the nucleation dynamics at boiling is performing both high-speed video visualization of boiling process close to a heating surface and investigation of non-stationary temperature field of a heater for further analysis of the local heat transfer characteristics under single vapor bubbles.

In this paper, with the use of above-mentioned high-speed video recording and IR thermography from the bottom side of a transparent heater, evolution of vapor bubbles, microlayer region, as well as the dry spots bounded by the contact line, and thermal characteristics at pool boiling of water and ethanol was studied in detail. Furthermore, behavior of the liquid-vapor system close to the heating surface at boiling was studied in a wide range of input heat fluxes.

## 2. Experimental setup and techniques

### 2.1. Experimental setup and test section

A schematic diagram of setup for pool boiling experiments is presented in Fig. 1. This setup consists of two sealed cylindrical

vessels made of stainless steel. To maintain a constant temperature of a working liquid, the boiling chamber was mounted in isothermal bath with two tubular heating elements (pre-heaters) with the total power of 2.4 kW. Water temperature in the isothermal bath was controlled using an electronic temperature controller. The working volume of boiling chamber is  $2.5 \times 10^{-3} \text{ m}^3$ . Temperature in boiling chamber and isothermal bath ( $T_1$  and  $T_2$  in Fig. 1) was measured using K-type thermocouples (chromel-alumel thermocouples). Constant atmospheric pressure in the boiling chamber was maintained with the use of vapor condenser with water cooling and was controlled by pressure sensor with accuracy of  $\pm 0.25\%$ .

As the working liquids in the present study were used deionized water produced by Direct-Q 3 UV water purification system and ethanol (96.6%) at saturation line (100 and 78 °C, respectively). In the experiments 1-μm-thick films of indium-tin oxide (ITO), vacuum deposited onto 400-μm-thick sapphire substrates, were used as the heaters. Fabricated samples had an electrical resistance of 2–3 Ohms and the heating area of  $20 \times 20 \text{ mm}^2$ . The surface roughness ( $R_a$ ) of the sapphire substrate was less than 1 nm according to the manufacturer (Hong Yuan Wafer Tech Co). The contact angle of the smooth sapphire substrate was 60° for deionized water and less than 10° for ethanol.

The main advantage of using ITO as a heater material in experiments on investigation of integral and local characteristics of heat transfer at nucleate boiling is its transparency in the visible spectrum (380–750 nm) and opacity in the mid-IR spectrum (3–5 μm). At the same time, sapphire transmission in the wavelength range of 0.3–5 μm exceeds 80%. The combination of these properties makes it possible to measure non-stationary temperature field on the ITO film surface by infrared camera and visually record vapor bubbles dynamics and liquid-vapor system structure directly on the sapphire substrate by high-speed video camera. Therefore, such construction of the heating element was recently widely used for pool boiling experiments [12,15,37].

It is known that intensity of heat transfer and critical heat flux at liquid boiling depends on the wall thickness. To compare our experimental data with the data of other authors obtained on thick-walled heaters and theoretical models correctly, the heating element should satisfy condition  $\delta \geq h_{av}$ , where  $h_{av}$  is the cooling depth or “the depth of penetration of temperature fluctuations” [22]. An estimate of the cooling depth, performed according to [44], taking into account the experimental data on the nucleation site density, bubble growth time and its departure diameter, showed that the heating element used in the experiments can be considered as thick-walled heater ( $\delta/h_{av} \sim 3$ ). Samples were resistively heated (Joule heating) by a DC power supply Elektro Automatik PS 8080-60 DT via thin silver electrodes vacuum deposited onto the ITO film. To determine the heat release rate for given current  $I$ , voltage  $V$  was measured on the heater with the use of APPA 109N digital multimeter. The heat flux density was calculated as  $q = V \cdot I / A$ , where  $A$  is the area of heater surface. The error in measuring the heat flux density is made up of the errors in measuring the voltage in the working section, current and surface area, and does not exceed 3%.

### 2.2. Video and infrared high speed visualizations

To visualize boiling process with high spatial and temporal resolutions digital video camera Vision Research Phantom v.7.0 with frame rate up to  $20 \cdot 10^3$  FPS was used. Visualization was performed from the bottom side of the transparent heater, as it is shown in Fig. 1. To study in detail evolution of the microlayer and dry spot regions, Nikon 105 mm f/2,8G macro lens was used in the work. The maximum spatial resolution of video recording in the experiments was 33 μm/pixel.

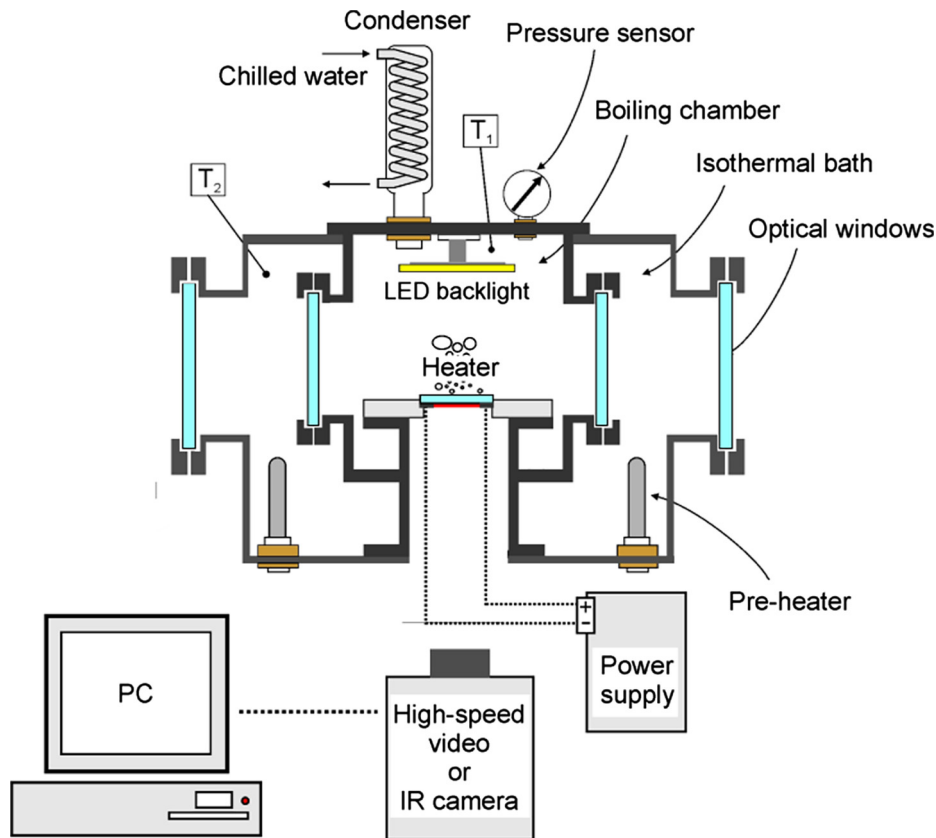


**Fig. 1.** Scheme of experimental setup.

In the experiments high-speed thermographic camera FLIR Titanium HD 570 M was used to measure the non-stationary temperature field of the heating surface. As configured for this study, the thermographic camera had a frame rate of 1000 FPS and maximum resolution of 150  $\mu\text{m}/\text{pixel}$ . For correct measurement of the heaters temperature field by thermographic camera, preliminary calibration procedure was performed before each series of experiments. The boiling chamber was filled with deionized water at room temperature ( $25^\circ\text{C}$ ) and then it was heated with  $3^\circ\text{C}$  increment up to approximately  $100^\circ\text{C}$  by pre-heaters mounted in outer isothermal bath. The temperature of the heater surface was monitored using platinum resistance thermometer HEL 700, which was mounted on the sapphire substrate near with ITO film. The temperature field also was monitored using the thermographic camera from the bottom side of the heater. Based on the results of the experiments, the calibration dependencies of the camera digital level on the surface temperature were plotted and then used in data analysis. As a result, the total uncertainty of the temperature measurements in the experiments did not exceed  $1^\circ\text{C}$ .

Due to high thermal conductivity ( $k = 25 \text{ W/m}\cdot\text{K}$ ) and small thickness of the sapphire substrate, the temperature on its surface was assumed to be equal to the temperature of the ITO film recorded by thermographic camera. However, in order to increase the thermal resolution of the thermographic recording, experiments on boiling of water and ethanol directly on the surface of the ITO film (the heating sample was turned upside down) were also carried out.

aged over recording time of 10 s and surface area at different heat flux density. Corresponding curves for water and ethanol, as well as experimental data of other authors are presented in Fig. 2. Calculations by Rohsenow correlation [45] also are shown in the figure for comparison. Analysis of the results shows that calculated data, as well as experimental data of [46,47] obtained at water and ethanol boiling on copper engineering surfaces, do not agree with data, obtained in the present study at boiling on the sapphire surface. The reason is that Rohsenow correlation contains empirical constant  $C_{sf}$  and extremely sensitive to it. In the present paper,  $C_{sf}$  values were taken on the basis of literature analysis 0.013 for water [45] and 0.0026 for ethanol [48]. In these studies  $C_{sf}$  values were obtained by generalization of the experimental data, obtained at pool boiling on engineering surfaces. At the same time it is well known that boiling heat transfer coefficient (HTC) is extremely sensitive to a heating surface roughness. Therefore contradiction observed in Fig. 2 can be related to the fact that used sapphire surface is ultra-smooth compared with engineering surfaces. In particular, this is confirmed by comparison of the experimental data with results of Yao et al. [49] and Nishio and Tanaka [40], obtained at water boiling on the polished silicon surface and at ethanol boiling on the sapphire surface with roughness parameters about nanometers. As it can be seen from the Fig. 2, obtained in these papers data are close to the present work results.

### 3.2. Vapor bubble dynamic at low heat fluxes

At the next stage the single vapor bubble growth was studied with the use of high speed video macrovisualization. Fig. 3 shows obtained frames of nucleation, growth and further departure of the vapor bubble at water boiling at relatively low heat flux ( $q = 31.5 \text{ kW/m}^2$ ). From the pictures at the initial time moments it can be seen that under the vapor bubble there are two regions:

## 3. Results and discussion

### 3.1. Boiling curves

To construct boiling curves experimental data on the heating surface temperature obtained using IR-thermography were aver-

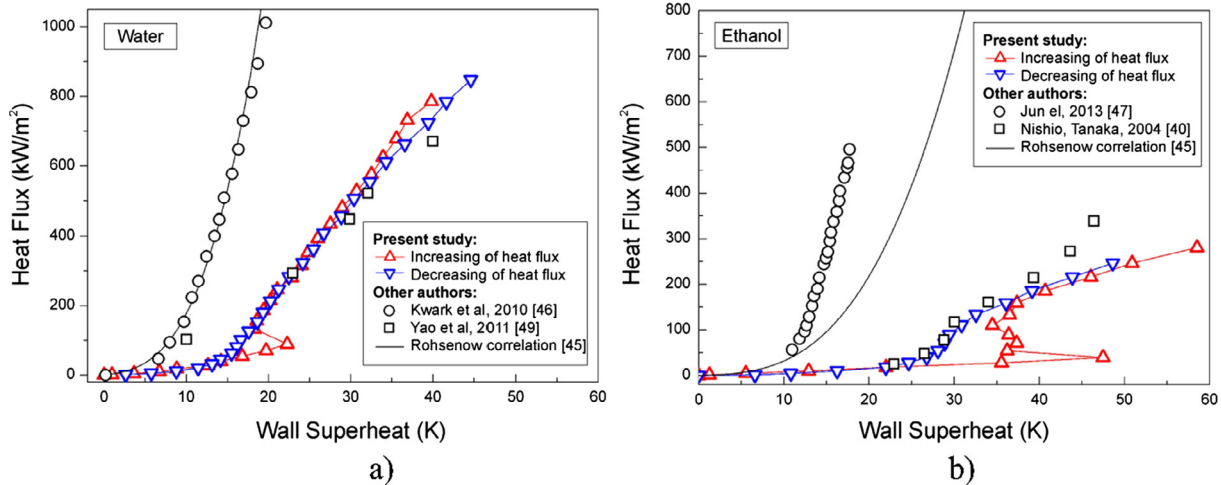
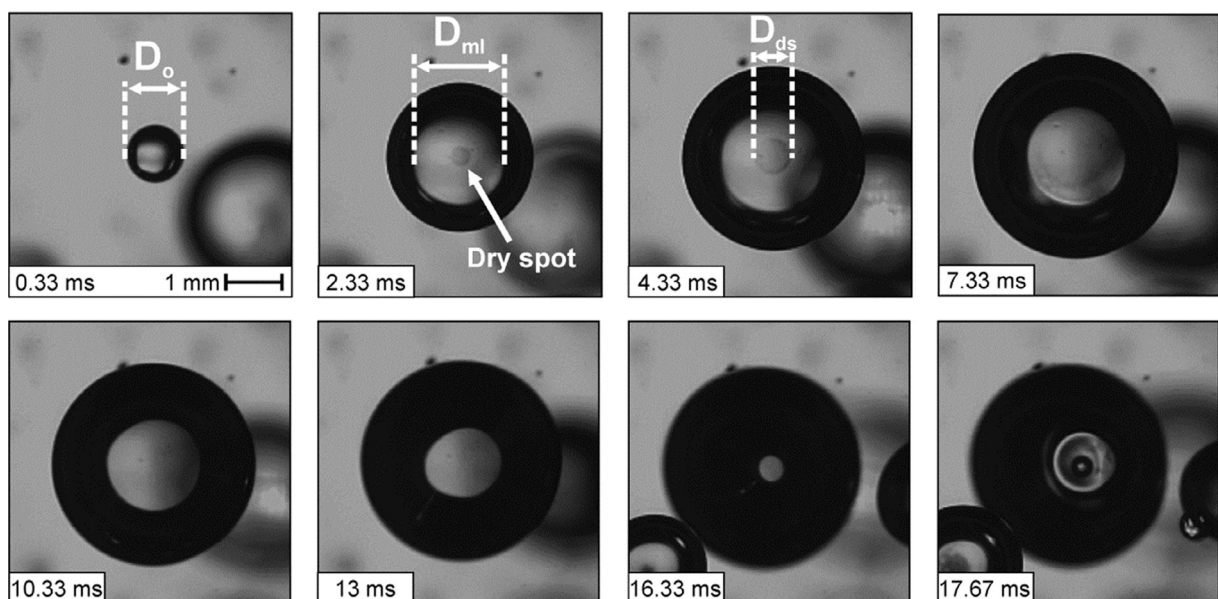


Fig. 2. Boiling curves of saturated (a) water; (b) ethanol.

the area bounded by the dark line corresponds to the bubble outer boundary and the bright area corresponds to the microlayer region. The fact that the bright area at video recording is the region of microlayer evaporation was shown early by Buongiorno et al. [12] on the basis of synchronized video and IR thermography data comparison. After the bubble appearance and its rapid growth, the dry spot bounded by the triple contact line is forming in the nucleation site in a short time (up to 1 ms), as it could be seen from Fig. 3. After that, dry spot area expands due to the intense evaporation of liquid from the microlayer surface. After the complete microlayer evaporation the bubble departure stage begins, during which the size of the contact line decreases. The moment of the vapor bubble departure corresponds to the collapse of the contact line. A similar behavior of growth and departure of vapor bubbles was also observed at ethanol boiling at low heat fluxes.

Based on the analysis of the high speed visualization results, experimental data on evolution of outer diameter, microlayer region and size of the dry spot for single vapor bubble at water and ethanol boiling were obtained (Fig. 4). Vertical lines on the plots correspond to the moments of complete microlayer evapora-

tion and vapor bubble departure. As it can be seen from the picture, the moment, at which boundary of the dry spot reaches the microlayer region boundary, corresponds to the beginning of the contact line area reducing. In other words, the vapor bubble departure stage at boiling on the ultra-smooth heating surface begins after the complete evaporation of liquid in the microlayer region. Analysis of obtained data shows, that dynamic of a vapor bubble growth and departure has a similar behavior at water and ethanol boiling. However, as can be seen from Fig. 4, at ethanol boiling, in contrast to water boiling, after the complete microlayer evaporation the bubble outer diameter continues to grow and the volume of vapor bubble may increase up to 2 times. This distinction can be explained as follows. Analysis of IR recording data on the temperature field of the heating surface, performed in previous studies [17,50], shows that at ethanol boiling the temperature of the surface in the nucleation site area up to the moment of the complete microlayer evaporation may significantly exceed saturation temperature. Therefore, in the case of ethanol boiling, evaporation takes place over the whole surface of vapor bubble due to the enthalpy abundance of surrounding superheated liquid. As a result,

Fig. 3. Frames of high-speed macro video recording of single vapor bubble dynamics at water boiling ( $q = 31.5 \text{ kW/m}^2$ ).

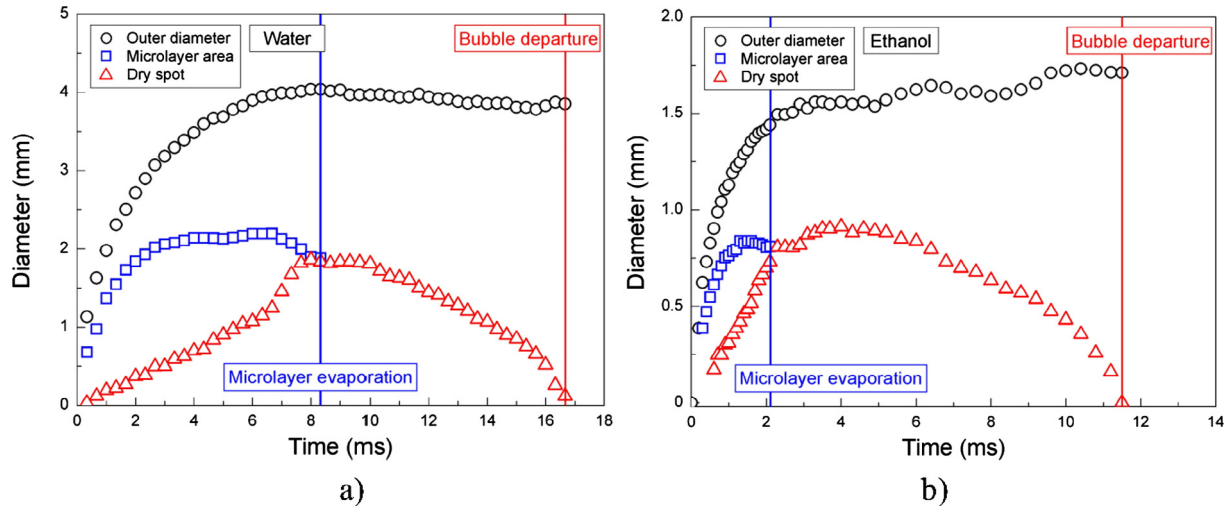


Fig. 4. Evolution of the outer diameter of a single bubble, the region of a microlayer and a dry spot at boiling of (a) water ( $q = 31.5 \text{ kW/m}^2$ ); (b) ethanol ( $q = 33.6 \text{ kW/m}^2$ ).

bubble size continues to increase even after the complete evaporation of liquid microlayer. Furthermore, Fig. 4 shows that ratio of the bubble departure time to the bubble growth time for ethanol is significantly greater than at water boiling.

Also in the study, growth and departure dynamics for ensemble of bubbles formed in different sites of the heating surface at a given heat flux, was analyzed. As can be seen from Fig. 5, growth rates and maximum bubbles sizes before departure can differ from each other for vapor bubbles formed in different sites (e.g. for water boiling the difference in bubble departure diameter might be up to 2 times). This is due to the following fact. Analysis of data on evolution of the surface local temperature under individual nucleation sites obtained with the use of IR thermography (Fig. 6) shows that the bubble nucleation temperature can significantly vary for different sites. This means that the heat necessary for the activation of vapor bubbles in different nucleation sites can vary depending on local features of a heating surface. Also, for comparison, the growth rate of vapor bubble on a heating wall was calculated by Labuntsov-Yagov correlation [51] for different Jacob numbers, corresponding to the minimum and maximum local wall superheat in nucleation sites at the moment of vapor bubble appearance:

$$D_0(t) = 2(\gamma Ja + \sqrt{\gamma^2 Ja^2 + 2\beta Ja})\sqrt{\alpha t}; \gamma = 0.3; \beta = 6. \quad (1)$$

As can be seen from Fig. 5, experimental data, obtained at water and ethanol boiling, are bounded by calculation curves. The analysis of experimental data shows, that wall superheat increase (Jacob number value increase) leads not only to an increase of vapor bubbles growth rates, but also to increase of their departure diameters. Therefore, for theoretical description of vapor bubbles evolution it is necessary to take into account both the forces of surface tension and buoyancy, and the excess enthalpy of a liquid. Today there are some semi-empirical models [52–56] constructed by generalization of experimental data, which present dependences for vapor bubble departure diameter, taking into account Jacob number.

Fig. 7 shows the experimental data on evolution of diameters of vapor bubbles and microlayer regions in dimensionless coordinates (the outer diameter of vapor bubble and the size of microlayer region were divided by the value of the bubble departure diameter; time was divided by the time of vapor bubble departure from the heating surface). As can be seen from the plots, data in dimensionless coordinates on bubble growth dynamic and evolution of the microlayer region, obtained for different nucleation sites and heat flux densities, almost coincide with each other.

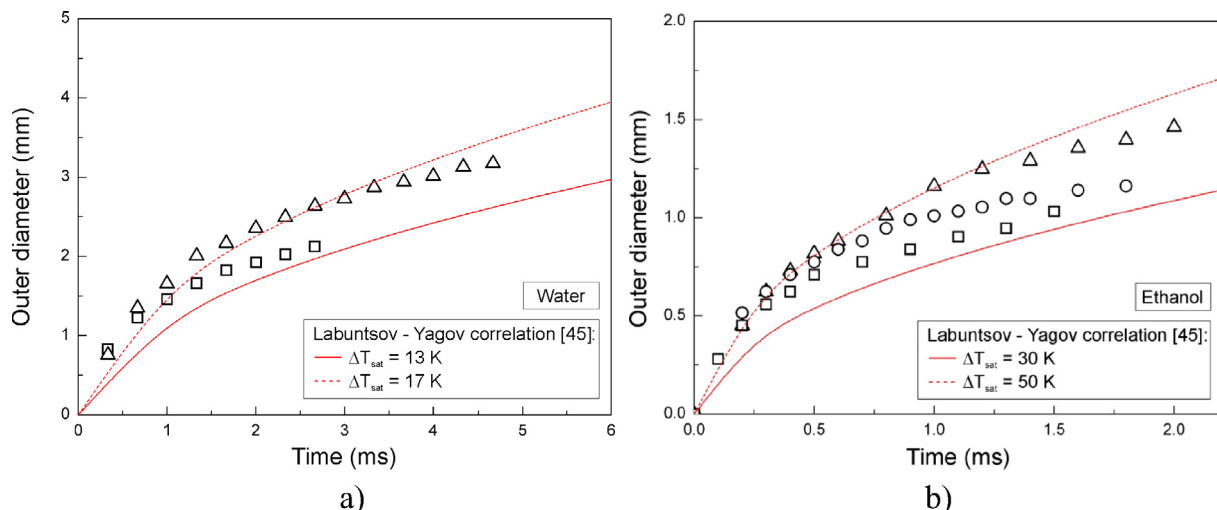
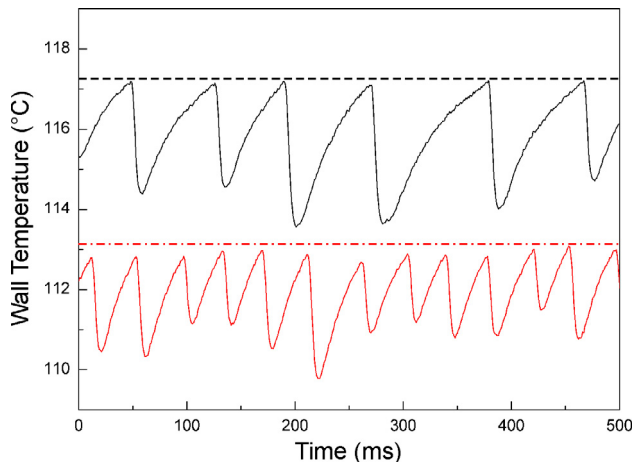


Fig. 5. Evolution of the outer diameter of vapor bubbles formed in different nucleation sites at (a) water ( $q = 45.6 \text{ kW/m}^2$ ); (b) ethanol ( $q = 33.6 \text{ kW/m}^2$ ).



**Fig. 6.** The local temperature of a heating surface under different nucleation sites at water boiling ( $q = 45.6 \text{ kW/m}^2$ ).

The size of the microlayer region is related to the bubble outer diameter and its maximum size both for water and ethanol boiling reaches the value of  $D_{dep}/2$ . Moreover the time of complete microlayer evaporation at water boiling varies in the range of  $t/t_{dep} = 0.4\text{--}0.5$  and the outer diameter already reaches its maximum value at  $t/t_{dep} = 0.3\text{--}0.4$ . In the case of ethanol boiling relative time of the bubble growth  $t/t_{dep}$  is  $0.1\text{--}0.2$ . Also at the bubble departure stage the bubble diameter increases due to the evaporation of ethanol from the whole bubble surface.

### 3.3. Dry spot growth rate

Experimental data on the evolution of dry spots in the base of the bubbles formed in different nucleation sites with different growth rates at water and ethanol boiling at the given heat flux are presented in Fig. 8a. The figure shows that the radius of the triple contact line linearly increases in time, i.e. the dry spot growth rate for each vapor bubble is constant. Moreover, difference in growth rate values is negligible for vapor bubbles, formed in different nucleation sites. Also it is seen that at similar heat fluxes the growth rate of the dry spot is higher for ethanol in comparison with water boiling, which is related to the lower value of the latent heat of vaporization of ethanol. Fig. 8b represents the dependence

of dry spot growth rate on the heat flux density at water boiling. It can be seen from the figure that value  $dR_{ds}/dt$  grows linearly with the heat flux increasing. At heat fluxes near the CHF point, dry spot growth rate increases up to  $0.6 \text{ m/s}$ .

With the use of heat balance equation it becomes possible to estimate a time of complete microlayer evaporation  $t_{ev} = \rho_l h_{fg} \delta_{ml} / q_{ev}$ . This estimation is based on the assumption that a total heat flux from a heating surface to the microlayer completely expends in a liquid evaporation and its value is equal to the input heat flux. It is also assumed, that a liquid in the microlayer is motionless, which means that the change of the liquid layer thickness  $\delta_{ml}$  is driven by the evaporation. For estimations, maximum microlayer thickness value was accepted equal to  $4 \mu\text{m}$  for water and  $3 \mu\text{m}$  for ethanol on the basis of the data obtained by the laser interferometry method [14,20,57]. Based on the results of estimations, the complete evaporation of the liquid microlayer at boiling in the region of low heat fluxes ( $100 \text{ kW/m}^2$  for water and  $50 \text{ kW/m}^2$  for ethanol) takes about  $90 \text{ ms}$  for water and  $40 \text{ ms}$  for ethanol. At the same time analysis of obtained experimental data shows, that corresponding values are  $9 \text{ ms}$  and  $2 \text{ ms}$ , respectively. Such significant difference can be explained by the fact that a local heat flux density in the region of microlayer exceeds by several times an average input heat flux.

The value of local heat flux in the microlayer region ( $q_{ml}$ ) can be estimated based on the assumption that the heat flux is defined by the thermal conductivity of a liquid layer in this area. Therefore time of complete evaporation of the liquid microlayer can be written as  $t_{ev} = \rho_l h_{fg} \delta_{ml}^2 / 2k(T_w - T_{sat})$ , where  $T_w$  values are known from the analysis of IR thermography data. Complete evaporation times calculated using this expression ( $6 \text{ ms}$  for water and  $1 \text{ ms}$  for ethanol) are closer to experimental data. Estimation of the local heat flux density shows that its average value for water should be not less than  $1400 \text{ kW/m}^2$ . At the same time average values of  $q_{mb}$ , which were reconstructed from IR thermography data by solving inverse nonstationary heat equation [13,14,16,17], do not exceed  $1000 \text{ kW/m}^2$ .

To explain possible reasons of such contradiction, results obtained by Jung and Kim [16] can be used. In this study authors calculated local heat flux in the microlayer region in three ways: as the amount of heat which provides the rate of changing microlayer thickness, observed using laser interferometry data; by solving nonstationary heat equation, on the base of the data on surface temperature field, obtained using IR thermography; by solving one-dimensional stationary heat equation for the liquid layer with

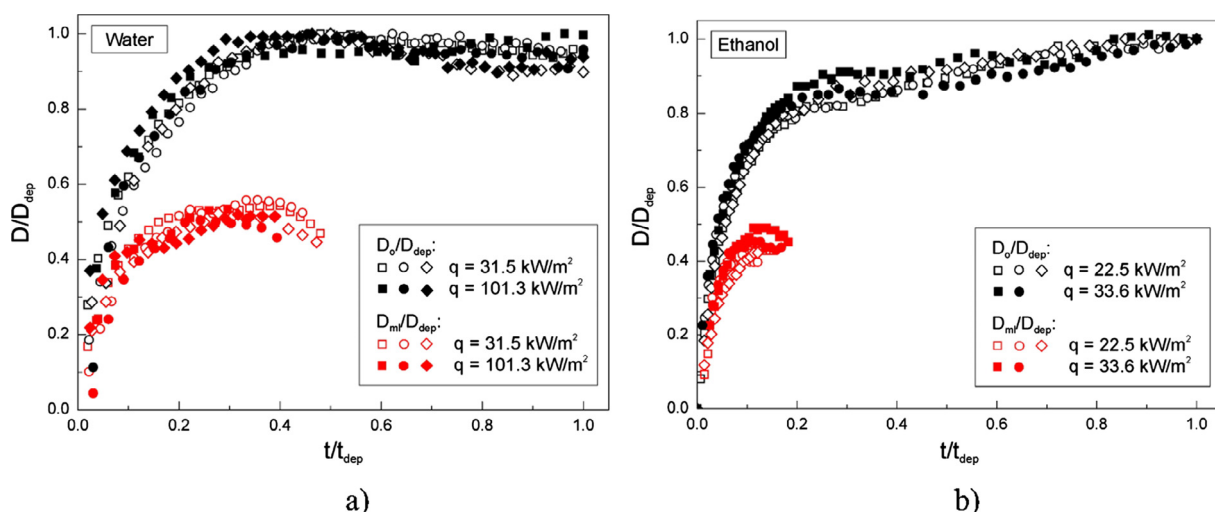


**Fig. 7.** Dynamics of vapor bubbles and the microlayer region for various nucleation sites and heat flux densities at boiling of (a) water; (b) ethanol.

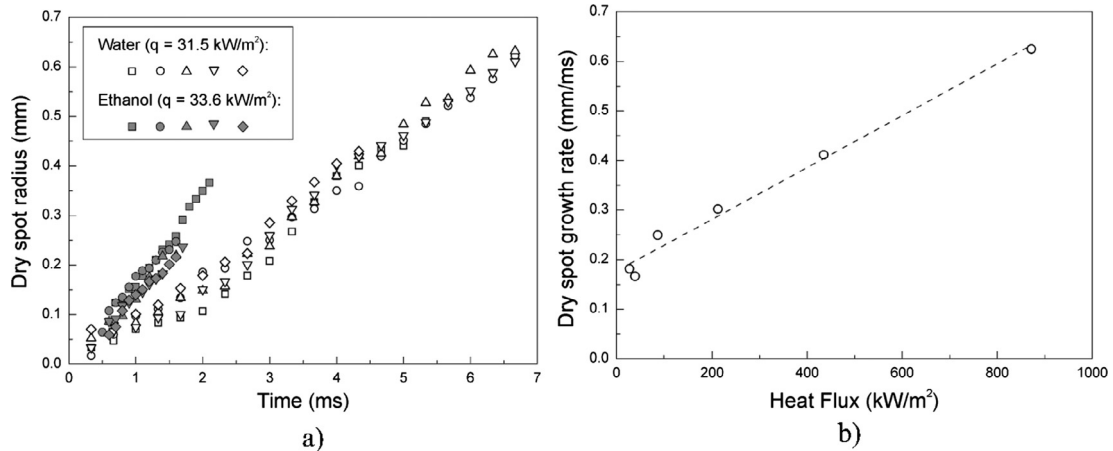


**Fig. 8.** (a) Dependence of the dry spot radius on time for different nucleation sites at water and ethanol boiling; (b) Dependence of dry spot growth rate on heat flux density at water boiling.

a given thickness. Authors showed that values obtained by first two ways were in a good agreement with each other, while third way gave much higher value. It means, that there is a physical effect (that is different from thermal conductivity of a liquid layer), which limits heat transfer from a superheated surface to a vapor bubble through a liquid microlayer.

Giustini et al. [58] with the use of experimental data obtained by Jung and Kim [14,16] showed that heat transfer through a microlayer depends on the evaporative resistance, which is related with molecular dynamics of the evaporation process in the liquid-vapor interface. Thus, for an accurate description of the microlayer evolution it is necessary to take into account together molecular effect (connected with evaporation from the surface of the microlayer), thermal conductivity of the liquid layer and a real shape of the microlayer.

#### 3.4. The dynamics of vapor bubbles at moderate and high heat fluxes (fully developed nucleate boiling regime)

In this section we tried to analyze the behavior of two-phase system close to a heating wall at pool boiling of water and ethanol in the range of moderate and high heat fluxes. The frames of high-speed video recording of water boiling at heat flux densities  $q = 435 \text{ kW/m}^2$  and  $872 \text{ kW/m}^2$  at different moments are presented in Fig. 9. From the analysis of video data, it is seen that at moderate heat fluxes (Fig. 9a), similar to the boiling at low heat fluxes, it is possible to clearly distinguish the individual vapor bubbles on the surface and the triple contact line in their base during dry spots formation. According to the sequence of video frames shown in Fig. 9a, after the appearance of vapor bubbles they quickly lose their symmetrical shape ( $t = 2\text{--}5 \text{ ms}$ ). As a result of the relatively high density of nucleation in most cases, the moment of detachment of individual vapor bubbles is preceded by the stage of merging of neighboring vapor bubbles, as it is evident from the last frame ( $t = 5 \text{ ms}$ ) in Fig. 9a. Analysis of high-speed visualization of the process showed that one of the reasons for the loss of the symmetrical shape of growing bubbles is the flow of liquid that occurs after detachment of individual or merged vapor agglomerates. Also after departure of vapor bubbles a rapid rewetting of the dry spots under them takes place. A further increase in the density of the heat flux leads to the fact that in the beginning of the growth stage neighboring vapor bubbles start to significantly influence on each other, merging and forming large vapor agglomerates as it is shown on Fig. 9b ( $t = 3\text{--}3.5 \text{ ms}$ ). It can be seen that for the overwhelming number of bubbles, the dynamics of vapor phase depar-

ture from the heating surface changes in comparison with low heat fluxes (described in Section 3.2). In particular, Fig. 9b ( $t = 3.5 \text{ ms}$ ) shows the appearance of new bubbles near the boundary of large vapor agglomerates formed by merging the neighboring vapor bubbles. On subsequent frames it can be seen that the outer boundary of new vapor bubbles at certain moment during the growth stage rapidly loses stability (Fig. 9b,  $t = 4.5 \text{ ms}$ ) and disappears in a short time (Fig. 9b,  $t = 4.7 \text{ ms}$ ). Such dynamics of the collapse of growing vapor bubbles is most likely caused by their merging with vapor clouds formed at some distance from the heating surface.

If we perform a comparative analysis of the growth rate  $u_g$  at given high heat flux and the ascent rate of a single vapor bubble  $u_a$ , calculated according to the estimated expression [59]:

$$u_a = 1.5 \sqrt[4]{\frac{g\sigma(\rho_l - \rho_v)}{\rho_l^2}}, \quad (2)$$

We obtain that at water boiling at high heat fluxes the value of  $u_g$  is more than four times greater than  $u_a$ . It should be noted that results calculated by (2) showed good agreement with the experimental data on the ascent rate of single bubbles obtained in [60] at saturated water boiling on a smooth tubular heater. At the same time, the analysis of growth time  $t_g$  and waiting time of new bubble appearance  $t_w$  are close to each other ( $t_g \sim 2 \text{ ms}$ ,  $t_w \sim 4 \text{ ms}$ ). As a result, floating vapor bubbles do not have enough time to move away from the heating surface during the period of  $t_g + t_w$  and merge with new growing bubbles, which results in a rapid loss of stability and collapse of the liquid-vapor interface of the growing vapor bubble. As a result of such merging at some distance from the heating surface, a region with a maximum void fraction, “vapor cloud”, or the so-called “vapor blanket” [31], is formed.

With the use of the data on growth rate and time become possible to estimate the distance from heating surface  $h = u_g \cdot t_g$ , on which described merging of bubbles with the overlying vapor blanket occurs. Such estimation also needs to take into account the shape asymmetry of the growing vapor bubble (the inequality of the diameter of a bubble base and its height), which was experimentally demonstrated by various authors by visualization of single vapor bubbles dynamics from the side of the heater [7–9]. In particular, Jung and Kim [14] showed that the bubble at boiling of water at atmospheric pressure has a flattened shape at the growth stage, and its height is 70–80% of the diameter. As a result, the value of  $h$  at  $q = 872 \text{ kW/m}^2$  is about 1 mm. Obtained results agree with the results of Iida and Kobayashi [32], who showed using

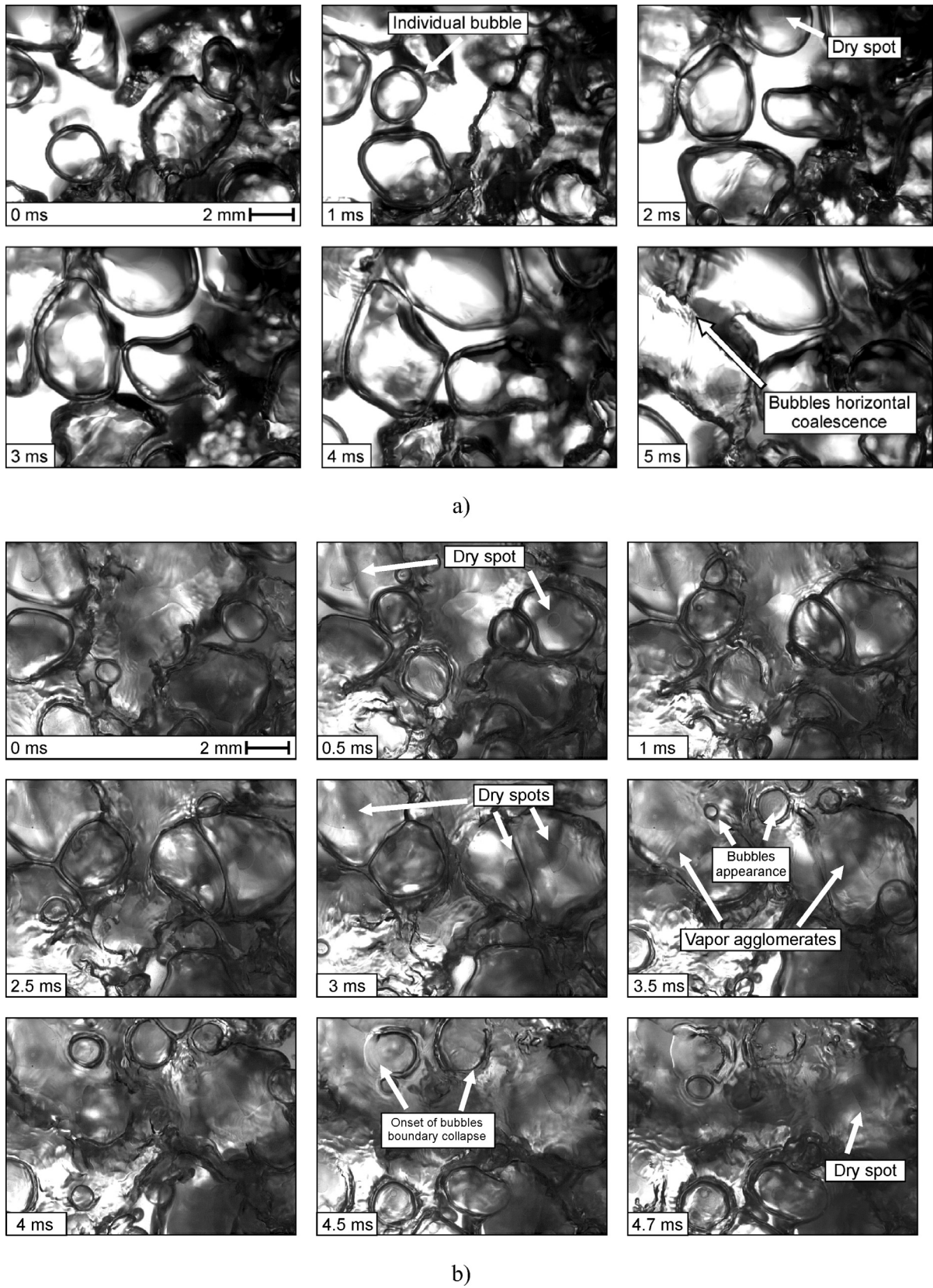


**Fig. 9.** Frames of high-speed visualization of evolution of vapor bubbles and dry spots at water boiling in the range of moderate and high heat fluxes. (a)  $q = 435 \text{ kW/m}^2$ ; (b)  $q = 872 \text{ kW/m}^2$ .

the probe method, that in the pre-crisis boiling mode of saturated water the maximum void fraction is 90% and is reached at distances up to 1 mm from a heating surface. Thus, at high heat fluxes due to the merging of growing and floating vapor bubbles near the heating surface, a vapor blankets are formed. These vapor clouds are fed by bubbles, which are formed in the same places and act as unsteady periodic vapor columns.

With the appearance of vapor bubbles, it is clearly seen formation of growing dry spots in their base, which are rapidly rewetted by surrounding liquid after vapor phase departure. However, in addition to single dry spots on the surface, the coalescence of neighbor spots and the formation of coagulated dry areas are also observed at high heat fluxes. Such large dry areas can exist on the surface for a relatively long time (up to 6 ms) before their rewetting (Fig. 9b). The above described dynamics of two-phase system close to a heating wall at water boiling at high heat fluxes is close to the experimental observations of Chu et al. [37]. In this work authors using total reflection technique at fully developed nucleate boiling of saturated water on the sapphire surface also observed the formation of large-scale dry area on the heater as the result of coalescence of individual dry spots. One of the conclusions of [37] is that the crisis phenomena development is an irreversible process, the catalyst of which is the appearance of non-wetting dry patch. The authors of [37] also proposed the possible mechanism of irreversible dry patch formation, in which the bubble nucleation activity in the wetting region plays an important role.

With the use of the high-speed thermographic recording, the evolution of the heater temperature field at water boiling in the region of moderate and high heat fluxes was also studied (Fig. 10). In these experiments, boiling was carried out directly on the ITO films. This allowed to substantially increase the temperature response and resolution at measuring the non-stationary temperature field of the heating surface in comparison with the boiling on the sapphire surface. Comparison of the results of high-speed video recording of developed boiling of water and ethanol on the smooth ITO film and sapphire surfaces showed that the dynamics of the two-phase system is practically the same, which makes correct further qualitative analysis of the IR thermography data. The analysis of the IR data showed that there are dark spots ("cold spots") and light areas bordered by a dark line on the surface. Cold spots are the temperature responses to the vapor bubbles appearance on the heating surface. Light areas bordered by a dark line are the responses to the growing vapor bubbles on the surface, where light areas are the regions of dry spots and dark line is an area of influence of liquid microlayer evaporation. Beginning of the blur of the dark line surrounding dry spot corresponds to the onset of bubble departure stage. Analysis also shows that at moderate heat fluxes the area of dry spots rapidly decreases on the departure stage. It is important to note that the temperature in the dry spot area is not much higher, than in other places of the wetted surface and the maximum size of dry spot does not exceed 3.5 mm, what agrees with the data of high-speed video recording.

Analysis of thermograms presented in Fig. 10b shows, that at boiling in the range of high heat fluxes the number of cold spots increases, which corresponds to increase of nucleation site density. In the overwhelming majority cold spots collapse in a short time (~2–3 ms) after the moment of their appearance and therefore the size of the dry spot area does not reach large scale in comparison with the case of boiling at moderate heat fluxes. At the same time, large dry areas form in some nucleation sites, as a result of the coalescence of neighbor vapor bubbles. Such coagulated dry spots in comparison with dry spots behavior at moderate heat fluxes are not rewetting for relatively long time. In particular, in the IR frames presented in Fig. 10b the life time of dry areas is about 6 ms. Moreover, the temperature in the area of dry spots during their life time increases and may exceed the average surface

temperature by 10–30 °C. Therefore, it is natural to assume that the onset of the boiling crisis, as it was described in many theoretical and experimental researches published recently, including visual studies, is nothing less than an unlimited increase in a dry spots area and an increase in temperature in this area up to the burning out of a heating element. In other words, the moment of the CHF is a moment of loss thermal stability of dry spots on a heating surface. In our opinion, the problem of stability of areas with deteriorated heat transfer affects many multiscale aspects of nucleate boiling, including heat transfer in the region of triple contact line, dynamics of two-phase layer near a heating surface, which determines the fluid inflow from a surrounding volume and the microhydrodynamics of the process and, accordingly, heat transfer in the macro- or microlayer regions. Certainly, this problem requires further theoretical comprehension to construct more universal solutions.

In the case of ethanol boiling in the range of moderate and high heat fluxes the boiling structure close to heating surface differs from water boiling. At ethanol boiling at moderate heat fluxes ( $q = 158 \text{ kW/m}^2$ ), as it is shown in Fig. 11a, there is simultaneously a large number of vapor bubbles that look like "vapor cells" (Fig. 11a,  $t = 0 \text{ ms}$ ). The average size of the observed "vapor cells" varies in the range from 0.7 to 2 mm. These vapor bubbles are demarcated by "liquid bulkheads", as shown in Fig. 11a ( $t = 1 \text{ ms}$ ), which resemble the so-called "plateau borders" in soap films. These bulkheads have almost the same transverse size of about 0.1 mm. However, similar to the case of water boiling in the region of moderate heat fluxes, merging of the neighboring vapor bubbles with formation of larger agglomerates is observed. A similar picture with patterns of liquid–solid contacts was also observed at ethanol boiling on the surface of a sapphire substrate by Nishio and Tanaka [40]. A detailed analysis of high-speed visualization data shows that a thin layer of liquid exists between the vapor formations – "cells" and the heating surface, and their connection with the surface is due to the dry spots. As a rule, new vapor bubbles appear in predetermined nucleation sites, mainly in the "liquid bulkhead" region, which is apparently due to the fact that in the region of a thin liquid film under "vapor cells", at such wall superheats, boiling is suppressed. During the bubble growth period dry spots are formed under them. At the next stage, a cascade coalescence of neighbor vapor bubbles, migrating along the heating surface, occurs, which results in the formation of large vapor agglomerates, whose size can reach ~3–4 mm. At the base of such vapor agglomerates, there may be several dry spots formed under different vapor bubbles. An interesting feature is that the rewetting of dry spots occurs either as a result of fluid flow during the coalescence of vapor bubbles, or at the departure of vapor formations from the surface.

The further increase in heat flux density ( $q = 246 \text{ kW/m}^2$ ) (Fig. 11b) leads to increase of the number of formed vapor bubbles per unit time and also to the increase of the size of large vapor agglomerates, which can reach up to 10 mm. An important difference from boiling at moderate heat fluxes is that in addition to the appearance of new bubbles in the "liquid bulkhead" region, the active nucleation is also observed in the region of thin liquid film under large vapor agglomerates. The growing vapor bubbles in thin liquid film quickly collapse (their lifetime does not exceed 1 ms) and dry spots remain in their place. Also dry spots under large vapor agglomerates appear as a result of merging with neighbor vapor bubbles. As a result, under the large vapor patterns, numerous dry spots with the size 0.3–1.2 mm exist. With the merging of several dry spots the larger dry zones with the size up to 4 mm can be formed, which exist on the surface until the beginning of the departure of the vapor phase and their further rewetting.

As it was mentioned above, the information about the distribution of local void fraction near a heating wall is also of fundamental

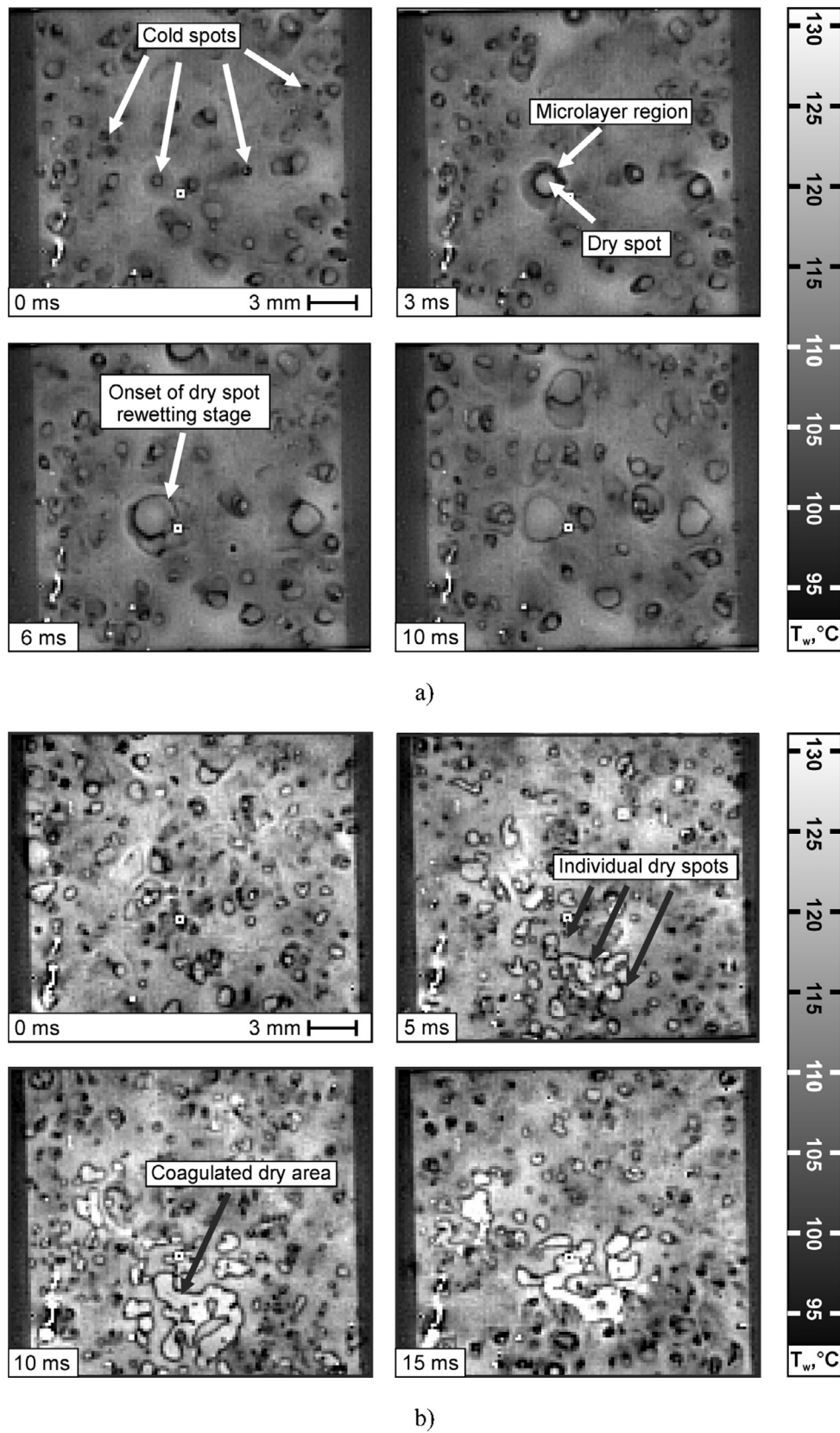


**Fig. 10.** Non-stationary temperature field on the heating surface at water boiling at different heat fluxes obtained by IR thermography. (a)  $q = 447 \text{ kW/m}^2$ ; (b)  $q = 850 \text{ kW/m}^2$ .

importance for understanding the evolution of a two-phase layer at fully developed nucleate boiling regime. The experimental results of the visualization of the ethanol boiling in this study made it pos-

sible to estimate the relative void fraction close to the heating surface. For this purpose, the ratio of the surface area under the vapor bubbles and agglomerates to the total area of the heater was calcula-

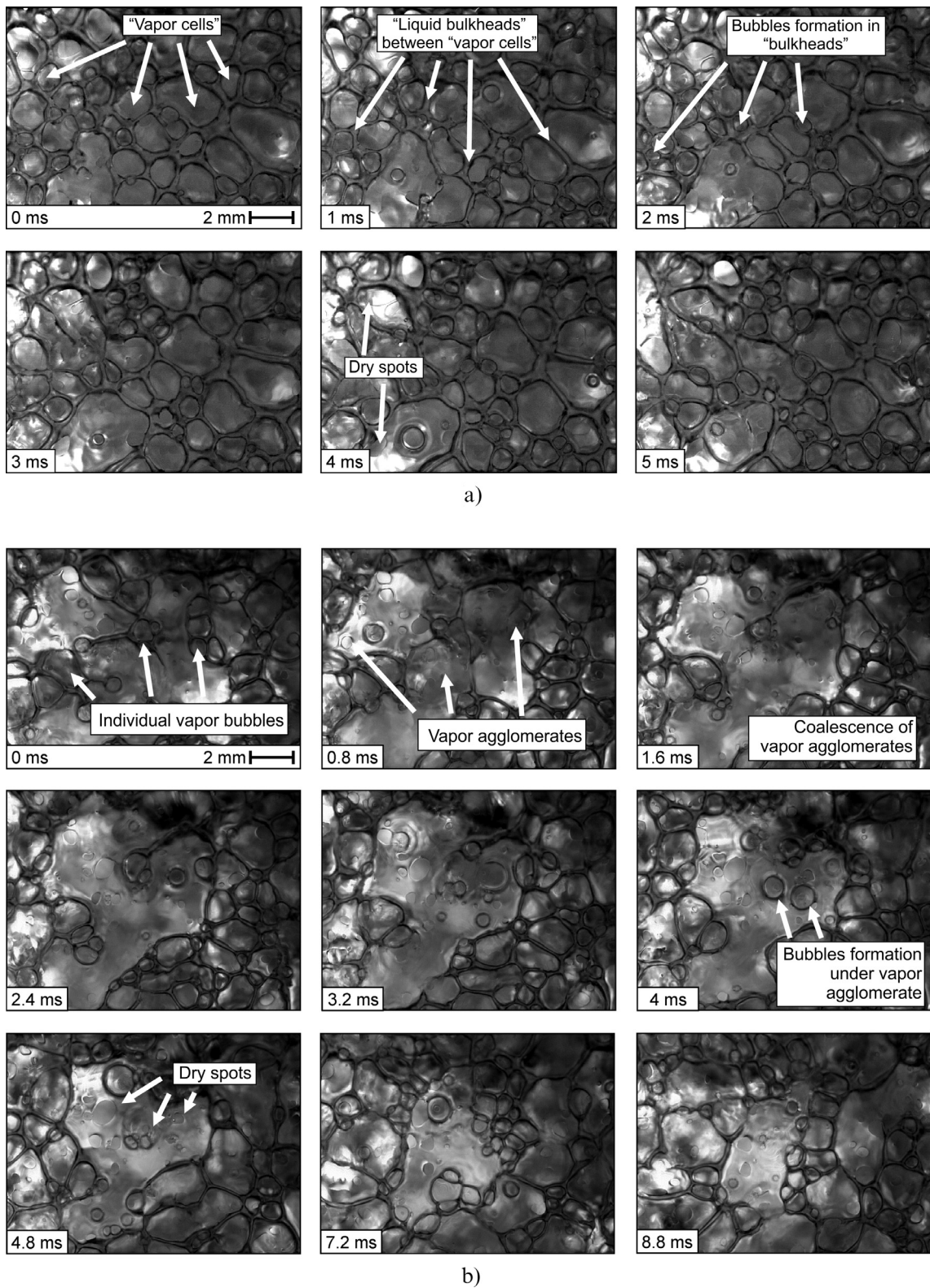


**Fig. 11.** Frames of high-speed visualization of evolution of “vapor cells” and dry spots at ethanol boiling in the range of moderate and high heat fluxes. (a)  $q = 158 \text{ kW/m}^2$ ; (b)  $q = 246 \text{ kW/m}^2$ .

lated for the selected frames. Averaging for each heat flux was carried out for 10 frames at different times. For more accurate calculation of the area under vapor agglomerates obtained frames were converted to a 2-bit format with the use of graphical editor software (Fig. 12). In the Fig. 13 the dependence of the relative value

of void fraction close to the surface at ethanol boiling on the dimensionless heat flux is presented. It can be seen from the graph that with increasing heat flux density, the relative void fraction increases and reaches a value of 0.8 at  $q/q_{CHF} \approx 0.6$ . Also for comparison experimental data of Nishio and Tanaka study [40], in

which the void fraction was analyzed directly on the surface of a sapphire substrate (i.e. the ratio of the dry spot area to the total heater area) at ethanol boiling up to the crisis phenomena development, are plotted in the Fig. 13. It can be seen that the data of the present study in the entire range of the heat fluxes are higher, than data of [40], which is related to the fact that the maximum void fraction at boiling is attained at some distance from a heating surface.

#### 4. Conclusions

In this paper the results of an experimental study of the features of the vapor bubbles dynamics at pool boiling of liquids with different physical properties in a wide range of heat fluxes up to  $q/q_{CHF} \approx 0.9$  are presented. The usage of high-speed experimental techniques including video macro-visualization and IR-thermography allowed not only to measure the outer diameter of vapor bubbles, but also to study in detail the evolution of the liquid microlayer region and the boundary of dry spots at the base of the bubbles and also to study the nonstationary temperature field of the heating surface. Based on the analysis of experimental results in the range of low input heat fluxes, following conclusions can be made:

1. The growth rate of outer diameter and the maximum sizes before departure of vapor bubbles can differ from each other for different nucleation sites on the heating surface due to the different activation temperature. At the same time the bubble growth dynamics and evolution of the microlayer region, obtained for different local regions and heat fluxes, almost coincide with each other in dimensionless coordinates;
2. The radius of triple contact linearly increases in time, i.e. the dry spots growth rate under vapor bubbles is constant and also increases with heat flux increasing at water boiling;
3. The vapor bubble departure stage at boiling of water and ethanol on the ultra-smooth heating surface starts after the complete evaporation of liquid in the microlayer region.

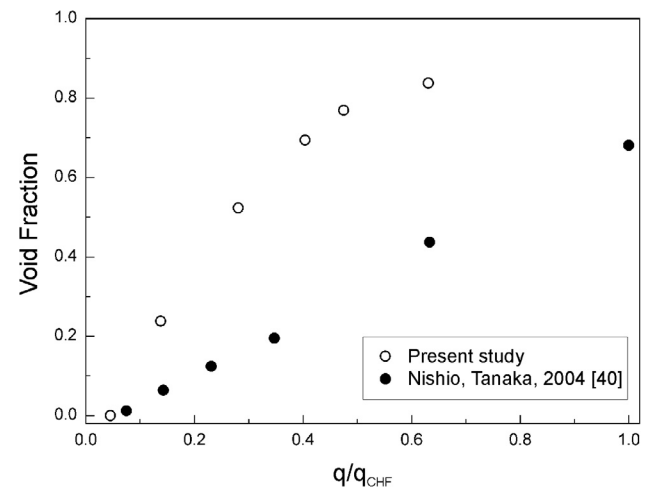


Fig. 13. The dependence of the relative value of void fraction close to the surface at ethanol boiling on heat flux.

An experimental observation the evolution of a two-phase systems and dry spots in the range of moderate and high heat fluxes shown:

1. The boiling structure near a heating surface at pool boiling of water and ethanol is different. At water boiling the stage of bubble departure observed at low heat fluxes, is absent at high heat fluxes. Vapor separation from the surface occurs as a result of coalescence of growing bubble with the upper vapor phase (in the form of large vapor agglomerates or “vapor clouds” and “blanket”, which is often considered in theoretical studies);
2. In the pre-crisis mode of nucleate boiling the large dry areas can formed due to merging of several dry spots formed under different nucleation sites and their life time and surface temperature under them can be much higher than at boiling in the region of moderate heat fluxes;

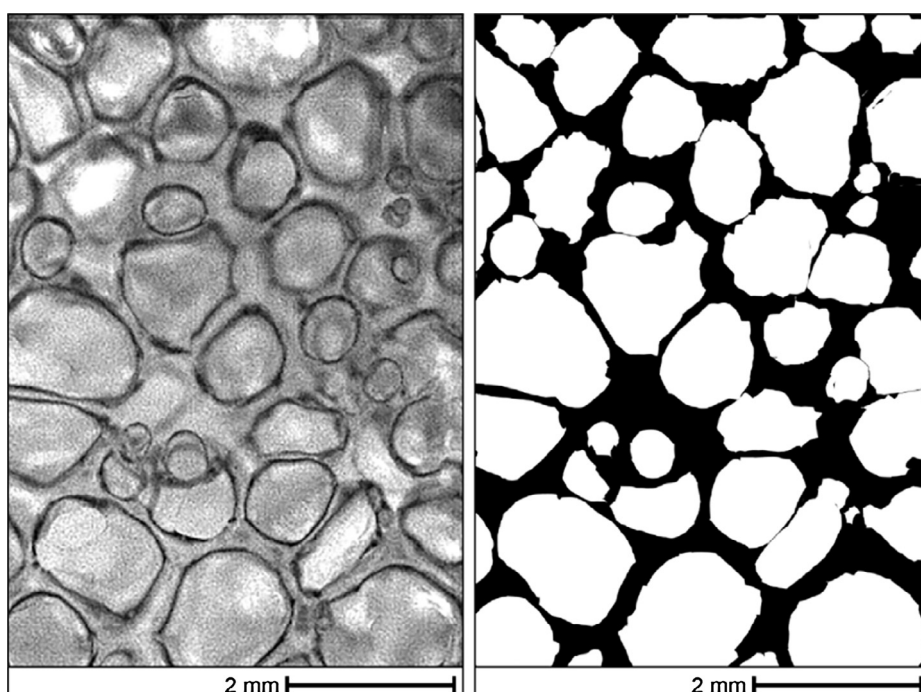


Fig. 12. The example of high-speed video frame processing for estimation the void fraction at ethanol boiling.

3. At ethanol boiling on the heating surface, migrating and cascadingly merging “vapor cells” are formed, separated by liquid bulkheads. The existence of a thin liquid film between the heating surface and the vapor cells was demonstrated;
4. At high heat fluxes the active nucleation in addition to the appearance of bubbles in the “liquid bulkhead” region also occurs in the region of thin liquid film, as a result of which, under the large vapor agglomerates, whose size can reach 4–5 cm, numerous dry spots can be observed;
5. New experimental data of relative void fraction close to heating wall at ethanol boiling were obtained. As a result, it was shown that the void fraction near the surface increases with heat flux increase and can reach a value of 0.8 at  $q/q_{CHF} \approx 0.6$ .

The experimental information obtained in the present study can be used in the future to formulate new theoretical approaches for describing main local boiling characteristics, including the evolution of various heat transfer areas under individual vapor bubble, evaporation rate of liquid microlayer, bubble departure diameter, nucleation frequency, local heat transfer rate, etc. Also obtained experimental information on the dynamics of two-phase system in the regime of fully developed nucleate boiling up to the CHF conditions can be used to construct more accurate physical picture for the theoretical description of heat transfer and CHF trigger mechanisms at boiling of liquids with different physical properties.

## Conflict of Interest

None declared.

## Acknowledgment

The reported study was funded by the Russian Foundation for Basic Research according to the research project № 17-08-01342. The part of the research was carried out according to the Program of Fundamental Scientific Research of the State Academy of Sciences for 2013–2020 (theme III.18.2.3, AAAA-17-117030310025-3). We express our gratitude to the Novosibirsk State University for giving us an access to the library.

## References

- [1] F.D. Moore, R.B. Mesler, The measurement of rapid surface temperature fluctuations during nucleate boiling of water, *AIChE J.* 7 (4) (1961) 620–624.
- [2] D.A. Labuntsov, Bubble growth mechanism on a heating surface, *J. Eng. Phys.* 6 (4) (1963) 33–39.
- [3] M.G. Cooper, A.J.P. Lloyd, The microlayer in nucleate pool boiling, *Int. J. Heat Mass Transf.* 12 (8) (1969) 895–913.
- [4] Z. Chen, A. Haginawa, Y. Utaka, Detailed structure of microlayer in nucleate pool boiling for water measured by laser interferometric method, *Int. J. Heat Mass Transf.* 108 (2017) 1285–1291.
- [5] T. Yabuki, O. Nakabeppe, Microlayer formation characteristics in pool isolated bubble boiling of water, *Heat Mass Transf.* 53 (5) (2017) 1745–1750.
- [6] S. Hänsch, W. Simon, The hydrodynamics of microlayer formation beneath vapour bubbles, *Int. J. Heat Mass Transf.* 102 (2016) 1282–1292.
- [7] D.B.R. Kenning, Optical studies of boiling heat transfer: insights and limitations, *Int. J. Heat Fluid Flow* 25 (2) (2004) 209–222.
- [8] S. Siedel, S. Cioulachtjian, J. Bonjour, Experimental analysis of bubble growth, departure and interactions during pool boiling on artificial nucleation sites, *Exp. Therm Fluid Sci.* 32 (8) (2008) 1504–1511.
- [9] M. Shoji, Y. Takagi, Bubbling features from a single artificial cavity, *Int. J. Heat Mass Transf.* 44 (14) (2001) 2763–2776.
- [10] T.G. Theofanous, J.P. Tu, A.T. Dinh, T.N. Dinh, The boiling crisis phenomenon: Part I: nucleation and nucleate boiling heat transfer, *Exp. Therm Fluid Sci.* 26 (6–7) (2002) 775–792.
- [11] T.G. Theofanous, T.N. Dinh, J.P. Tu, A.T. Dinh, The boiling crisis phenomenon: Part II: dryout dynamics and burnout, *Exp. Therm Fluid Sci.* 26 (6–7) (2002) 793–810.
- [12] C. Gerardi, J. Buongiorno, L.W. Hu, T. McKrell, Study of bubble growth in water pool boiling through synchronized, infrared thermometry and high-speed video, *Int. J. Heat Mass Transf.* 53 (19) (2010) 4185–4192.
- [13] I. Golobic, J. Petkovsek, D.B.R. Kenning, Bubble growth and horizontal coalescence in saturated pool boiling on a titanium foil, investigated by high-speed IR thermography, *Int. J. Heat Mass Transf.* 55 (4) (2012) 1385–1402.
- [14] S. Jung, H. Kim, An experimental method to simultaneously measure the dynamics and heat transfer associated with a single bubble during nucleate boiling on a horizontal surface, *Int. J. Heat Mass Transf.* 73 (2014) 365–375.
- [15] A.S. Surtayev, V.S. Serdyukov, M.I. Moiseev, Application of high-speed IR thermography to study boiling of liquids, *Instrum. Exp. Tech.* 59 (4) (2016) 615–620.
- [16] S. Jung, H. Kim, An experimental study on heat transfer mechanisms in the microlayer using integrated total reflection, laser interferometry and infrared thermometry technique, *Heat Transf. Eng.* 36 (12) (2015) 1002–1012.
- [17] V.S. Serdyukov, A.S. Surtayev, A.N. Pavlenko, A.N. Chernyavskiy, Investigation of local heat transfer in the contact line area under vapor bubbles at pool boiling, *High Temp.* 56 (4) (2018) 549–562.
- [18] H.H. Jawurek, Simultaneous determination of microlayer geometry and bubble growth in nucleate boiling, *Int. J. Heat Mass Transf.* 12 (8) (1969) 843–848.
- [19] C.M. Voutsinos, R.L. Judd, Laser interferometric investigation of the microlayer evaporation phenomenon, *J. Heat Transf.* 97 (1) (1975) 88–92.
- [20] L.D. Koffman, M.S. Plesset, Experimental observations of the microlayer in vapor bubble growth on a heated solid, *Int. J. Heat Mass Transf.* 5 (1983) 625–632.
- [21] M. Gao, L. Zhang, P. Cheng, X. Quan, An investigation of microlayer beneath nucleation bubble by laser interferometric method, *Int. J. Heat Mass Transf.* 57 (2012) 183–189.
- [22] V.A. Grigor'ev, Yu.M. Pavlov, E.V. Ametistov, Boiling of Cryogenic Liquids (in Russian), Energiya, Moscow, 1977, p. 288.
- [23] D. Bestion, Status and perspective for a multiscale approach to light water reactor thermalhydraulic simulation, in: Proceedings of the 14th International Topical Meeting on Nuclear Reactor Thermalhydraulics (NURETH-14), Toronto, Ontario, Canada, 2011, NURETH-14-632.
- [24] V.V. Yagov, Is a crisis in pool boiling actually a hydrodynamic phenomenon?, *Int. J. Heat Mass Transf.* 73 (2014) 265–273.
- [25] G. Liang, I. Mudawar, Pool boiling critical heat flux (CHF) – Part 1: review of mechanisms, models, and correlations, *Int. J. Heat Mass Transf.* 117 (2018) 1352–1367.
- [26] G. Liang, I. Mudawar, Pool boiling critical heat flux (CHF) – Part 2: assessment of models and correlations, *Int. J. Heat Mass Transf.* 117 (2018) 1368–1383.
- [27] R.F. Gaertner, Photographic study of nucleate pool boiling on a horizontal surface, *J. Heat Transf.* 87 (1965) 17–29.
- [28] D.B. Kirby, J.W. Westwater, Bubble and vapor behavior on a heated horizontal plate during pool boiling near burnout, *Chem. Eng. Prog. Sympos. Ser.* 61 (1965) 238–248.
- [29] H.J. Van Ouwerkerk, Burnout in pool boiling: the stability of boiling mechanisms, *Int. J. Heat Mass Transf.* 15 (1) (1972) 25–34.
- [30] Y. Katto, S. Yokoya, Principal mechanism of boiling crisis in pool boiling, *Int. J. Heat Mass Transf.* 11 (6) (1968) 993–1002.
- [31] Y. Haramura, Y. Katto, New hydrodynamic model of critical heat flux applicable widely to both pool and forced convection boiling on submerged bodies in saturated liquids, *Int. J. Heat Mass Transf.* 26 (3) (1983) 379–399.
- [32] Y. Iida, K. Kobayashi, Distributions of void fraction above a horizontal heating surface in pool boiling, *Bull. JSME* 12 (50) (1969) 283–290.
- [33] M. Buchholz, T. Lüttich, H. Auracher, W. Marquardt, Experimental investigation of local processes in pool boiling along the entire boiling curve, *Int. J. Heat Fluid Flow* 25 (2) (2004) 243–261.
- [34] H. Auracher, W. Marquardt, Heat transfer characteristics and mechanisms along entire boiling curves under steady-state and transient conditions, *Int. J. Heat Fluid Flow* 25 (2) (2004) 223–242.
- [35] A. Ono, H. Sakashita, Liquid-vapor structure near heating surface at high heat flux in subcooled pool boiling, *Int. J. Heat Mass Transf.* 50 (17–18) (2007) 3481–3489.
- [36] A. Ono, H. Sakashita, Measurement of surface dryout near heating surface at high heat fluxes in subcooled pool boiling, *Int. J. Heat Mass Transf.* 52 (3–4) (2009) 814–821.
- [37] I.C. Chu, H.C. No, C.H. Song, Visualization of boiling structure and critical heat flux phenomenon for a narrow heating surface in a horizontal pool of saturated water, *Int. J. Heat Mass Transf.* 62 (2013) 142–152.
- [38] S. Nishio, T. Gotoh, N. Nagai, Observation of boiling structures in high heat-flux boiling, *Int. J. Heat Mass Transf.* 41 (21) (1998) 3191–3201.
- [39] H.J. Chung, H.C. No, Simultaneous visualization of dry spots and bubbles for pool boiling of R-113 on a horizontal heater, *Int. J. Heat Mass Transf.* 46 (12) (2003) 2239–2251.
- [40] S. Nishio, H. Tanaka, Visualization of boiling structures in high heat-flux pool boiling, *Int. J. Heat Mass Transf.* 47 (21) (2004) 4559–4568.
- [41] J. Petkovsek, Y. Heng, M. Zupancic, H. Gjerkes, F. Cimerman, I. Golobic, IR thermographic investigation of nucleate pool boiling at high heat flux, *Int. J. Refrig.* 61 (2016) 127–139.
- [42] M. Shoji, A study of steady transition boiling of water: experimental verification of macrolayer evaporation model, in: Proceedings of Engineering Foundation Conference on Pool and External Flow Boiling, Santa Barbara, USA, 1992, pp. 237–242.
- [43] R. Hohl, J. Blum, H. Auracher, W. Marquardt, Characteristics of liquid–vapor fluctuations in pool boiling at small distances from the heater, in: Proceedings of 11th International Heat Transfer Conference, Kyongju, Korea, vol. 2, 1998, pp. 383–388.
- [44] I.I. Gogonin, The dependence of boiling heat transfer on the properties and geometric parameters of heat-transfer wall, *High Temp.* 44 (6) (2006) 913–921.

- [45] W.M. Rohsenow, A method of correlating heat-transfer data for surface boiling of liquids, *Trans. ASME* 74 (1952) 969–976.
- [46] S.M. Kwark, G. Moreno, R. Kumar, H. Moon, S.M. You, Nanocoating characterization in pool boiling heat transfer of pure water, *Int. J. Heat Mass Transf.* 53 (21–22) (2010) 4579–4587.
- [47] S. Jun, S. Sinha-Ray, A.L. Yarin, Pool boiling on nano-textured surfaces, *Int. J. Heat Mass Transf.* 62 (2013) 99–111.
- [48] P.K. Sarma, V. Srinivas, K.V. Sharma, V.D. Rao, Correlation for heat transfer in nucleate boiling on horizontal cylindrical surface, *Heat Transf. Eng.* 31 (6) (2010) 449–457.
- [49] Z. Yao, Y.W. Lu, S.G. Kandlikar, Effects of nanowire height on pool boiling performance of water on silicon chips, *Int. J. Therm. Sci.* 50 (11) (2011) 2084–2090.
- [50] A. Surtaev, V. Serdyukov, A. Chernyavskiy, Study of thermal behavior of microlayer under vapor bubble at liquid boiling, *EPJ Web Conf.* 159 (2017) 00051.
- [51] D.A. Labuntsov, V.V. Yagov, Growth rate of vapor bubbles in boiling, *Trans. Moscow Power Inst. Heat Mass Exchange Process. Apparatus.* 268 (1975) 3–15.
- [52] E. Ruckenstein, A physical model for nucleate boiling heat transfer, *Int. J. Heat Mass Transf.* 7 (2) (1964) 191–198.
- [53] R. Cole, W.M. Rohsenow, Correlation of bubble departure diameters for boiling of saturated liquids, *Chem. Eng. Prog. Sympos. Ser.* 65 (92) (1968) 211–213.
- [54] S.S. Kutateladze, I.I. Gogonin, Growth rate and detachment diameter of a vapor bubble in free convection boiling of a saturated liquid, *High Temp.* 17 (1979) 667–671.
- [55] V.P. Carey, *Liquid-Vapor Phase-Change Phenomena*, second ed., Taylor & Francis Group, New York, 2008, p. 742.
- [56] J. Kim, M.H. Kim, On the departure behaviors of bubble at nucleate pool boiling, *Int. J. Multiph. Flow* 32 (10–11) (2006) 1269–1286.
- [57] Y. Utaka, Y. Kashiwabara, M. Ozaki, Microlayer structure in nucleate boiling of water and ethanol at atmospheric pressure, *Int. J. Heat Mass Transf.* 57 (1) (2013) 222–230.
- [58] G. Giustini, S. Jung, H. Kim, S.P. Walker, Evaporative thermal resistance and its influence on microscopic bubble growth, *Int. J. Heat Mass Transf.* 101 (2016) 733–741.
- [59] D.A. Frank-Kamenetskiy, On the motion of bubbles and drops, in: *Proceedings of Scientific Institute No.1*, vol. 7, USSR, 1946, pp. 1–17 (in Russian).
- [60] A. Surtaev, D. Kuznetsov, V. Serdyukov, A. Pavlenko, V. Kalita, D. Komlev, A. Ivannikov, A. Radyuk, Structured capillary-porous coatings for enhancement of heat transfer at pool boiling, *Appl. Therm. Eng.* 133 (2018) 532–542.